*J. Earth Syst. Sci.* (2017) 126:50
DOI 10.1007/s12040-017-0825-z



# Provenance of coastal dune sands along Red Sea, Egypt

Samir M Zaid

*Department of Geology, Zagazig University, Zagazig 44511, Egypt.*
*e-mail: Samir_zaid75@yahoo.com*

MS received 14 November 2016; revised 9 January 2017; accepted 21 January 2017; published online 7 June 2017

Texture, mineralogy, and major and trace element geochemistry of 26 coastal dune sand samples were studied to determine the provenance and tectonic environment of two dune fields close to the beaches of Safaga (SF) and Quseir (QS) at the Egyptian Red Sea coast. Onshore winds generate fine, moderate, moderately-well to well-sorted, coarse-skewed to near-symmetrical dune sands with mesokurtic distributions. Winds pick up and transport grains from nearby beach sands and alluvial deposits into a wide Red Sea coastal plain at the border of the beach. The mineralogical (Qt–Ft–Lt) and geochemical composition of the sands, indicate that SF and QS coastal dune sands are mature and influenced by quartz-rich sands. The average CIA values in SF and QS coastal dune sands are low relative to the range of the PAAS, suggesting an arid climate and a low intensity of chemical weathering. The SF and QS coastal dune sand samples are plotted in the recycled orogen and partly in craton interior fields suggesting recycled older sedimentary and partly metamorphic-plutonic sources. The high content of quartz with shell debris and carbonates in coastal dune sands support the recycled sedimentary beach and alluvial sand sources. The dominance of heavy minerals like amphiboles (hornblende) and biotite in the coastal dune sands also supports the effect of metamorphic-plutonic source rocks. The new tectonic discriminant-function diagrams suggest that the coastal dune sands were deposited in a passive margin of a synrift basin. The results provide a good evidence for the extension in the Red Sea rift system during Oligocene-post Pliocene, which is consistent with the general geology of Egypt.

**Keywords.** Provenance; coastal dune sand; Red Sea; Egypt.

## 1. Introduction

The dune sands are widely distributed along the Egyptian Red Sea coast. Most of the large Red Sea coastal dune fields are formed at the mouth and adjacent to large wadis. These dunes occupy a narrow belt directly related to the sand supply and favourable wind regime. Sand beaches also contribute to the dune sediments. The coastal dune sands in desert environments are texturally and compositionally controlled by chemical and physical processes such as climate (precipitation, air temperature and wind actions), topography, mechanical transportation, fluvial and marine processes, and source composition (Carranza-Edwards 2001; Honda *et al.* 2004; Carranza-Edwards *et al.* 2009; Kasper-Zubillaga *et al.* 2013). Weathering products of the basement and Phanerozoic rocks are transported to the coast by torrent waters. The Red Sea coastal dune sands are generally in the form of parallel ridges with flat upper surfaces and continuous crests oriented more or less transverse to the dominant wind direction. This type of transverse dunes is associated with one dominant

effective wind (Fryberger 1979). These dunes have been mainly formed by the accumulation of sands behind vegetation or any other obstacles.

According to Egyptian Authority of Meteorology (1996) climate in the study area is arid with an average annual rainfall between 5 and 10 mm (Zaid 2002). The study area ranges in elevation between 0 m at the Red Sea coastal plain and 1040 m above the mean sea level at the highest peak in the Gebel Umm Ba'anib. This area has wind speed more than 21 knots. The onshore wind blowing directions are mainly north and northwest with frequency range 7–30% measured at Quseir. Average wave height is 2.2 m. The Red Sea coastal dunes are semimobile, vegetated, transverse and linear dune types (Mansour 1994). These dunes are stabilized, loose and Quaternary in age. The coastal dunes are in average 5.5 m long, 2.95 m wide and 0.8 m high. They reach a maximum elevation of 2 m above mean sea level at Quseir area. Despite their low elevation, the dunes represent a significant portion of the volume of sand comprising the coast.

Geomorphologically, the study area along the Red Sea coast of Egypt includes three major geomorphologic units: (1) denudation landforms consisting of mountains, and denudation hills; (2) deposition landforms consisting of alluvial fans and terraces, sandsheets, sand dunes and wadi deposits; and (3) denudation and/or depositional landforms consisting of coastal plain, shores, beaches lagoons, islands and coral reefs (Zaid 2002).

The study areas Safaga (SF) and Quseir (QS) field dunes (figure 1) are located along the Red Sea Coast. The area has been studied in terms of grain-size and detrital modes for provenance implications (Mansour and Sediek 1994; Mansour *et al.* 1997, 2000; Dar 1998, 2002; Mansour 1999; El-Taher and Madkour 2013; Ramadan and Zaid 2013). However, no sedimentological, modal analysis or geochemical research has been carried out in the Red Sea coastal dunes for provenance interpretation. Kasper-Zubillaga *et al.* (2013) studied the geochemistry of dune sands of Mexico and concluded that the dune sands are controlled texturally, compositionally and chemically by the nearby rivers.

The present paper aims to delineate the provenance of the Quaternary coastal dune sands along the Red Sea, Egypt, based on the sedimentology, modal analysis and geochemistry of major and trace elements of the sand samples collected from two dune fields close to the beaches of Safaga and Quseir. The study uses grain size parameters and petrographic and geochemical data as a contribution to the origin of coastal dunes.

## 2. Study area and geologic setting

The dune field area Safaga (SF) is located in the central Eastern Desert, Egypt (lat. 26°30′–26°50′N and long. 33°30′–34°00′E). The Red Sea coast bounded it from the east and Precambrian basement exposure to the west (figure 1). The investigated area is characterized by rugged mountainous relief of elevations up to 360 m (Gebel Nakheil), and steep slopes, especially along and near the northwestern and western parts of the Safaga and Gasus basin waterdivides (figure 1). The mountainous terrain occupies almost the entire Safaga basin, and is composed essentially of Precambrian crystalline basement rocks, dominated by granitoids of different compositions and ages, and less dominantly by metagabbros and Dokhan volcanics. The low-lying terrain, on the other hand, is narrow and covered by small outcrops of subdued sedimentary beds of Miocene and Pliocene ages, that overlie unconformably the mountain front of the highland, as well as surficial deposits of gravels, sands and clays of Quaternary age (Conoco 1987). The Red Sea basement terrains include the upstream of the catchment areas of rainfall, where running water flows to the Red Sea. Local fans are common at the foot slopes of the mountains.

The dune field area Quseir (QS) is located in the south-eastern desert, Egypt (lat. 25°50′–26°10′N and long. 33°40′–34°20′E, figure 1). The mountainous terrain occupies almost the entire Quseir el Qadim and Ambagi basins, and is characterized mainly by steep slopes of the issuing parts and mountainous relief up to 1200 m particularly near the western and southwestern part of the Quseir el Qadim and Ambagi waterdivides. The low-lying terrain forms a narrow strip (1–2 km wide) with gentle seaward slope, bordering the eastern flank of the highland. It is covered by small outcrops of low lying beds of Middle Miocene and Pliocene ages, as well as Quaternary fluviatile and coastal sediments. The mountainous terrain is a part of the Red Sea mountain chains and is composed of crystalline Precambrian basement complex. The rocks exposed include gneisses, metasediments, metavolcanics, serpintinites, metagabbros, and granitoid rocks (Conoco 1987).

Geologically, the study area along the Red Sea coast of Egypt includes three major lithologic

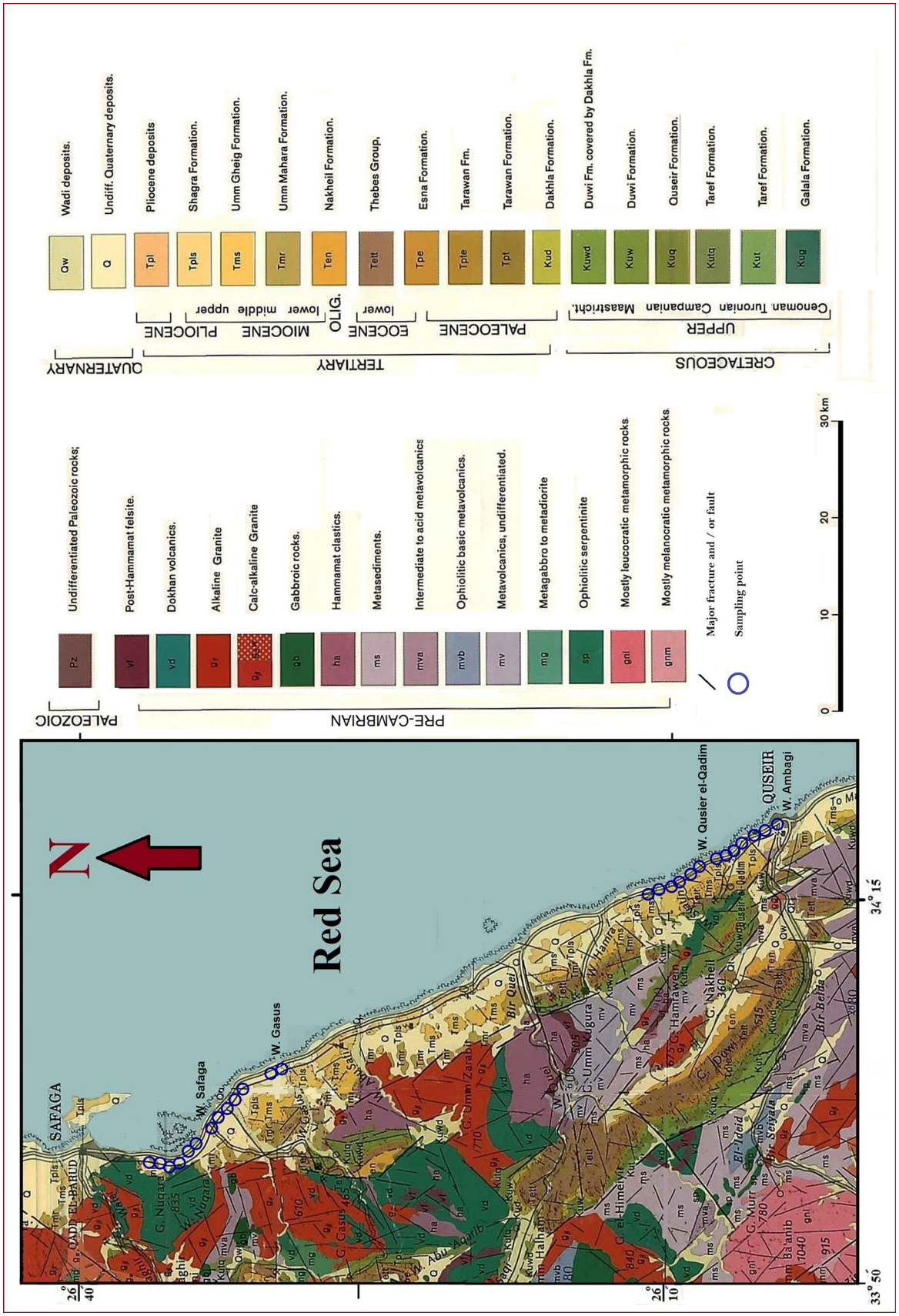


Figure 1. Geological map of the study area showing locations of point sampling (modified after Conoco 1987).

groups (Conoco 1987; figure 1): (1) a late Precambrian basement complex consisting of highly deformed volcanics and volcanogenic sediments metamorphosed to lower greenschist facies; (2) Cretaceous to early Eocene platform sediments consisting of up to 600 m of well-bedded sandstones, shales and limestones; and (3) Miocene to Recent Red Sea coastal plain sediments consisting of fanglomerates, marls, evaporites and calcareous reef deposits.

The Precambrian volcano-sedimentary units appear to have been deposited in an oceanic island-arc environment. Major granitic intrusions were syn- to post-tectonic. The unconformably overlying platform sediments are exposed as east-dipping tilted blocks and down-faulted inliers within the Precambrian basement (Ries *et al.* 1983). The Cretaceous to early Eocene platform sediments, deposited at the margin of the developing Red Sea rift, thicken and dip eastward towards the rift axis. Abrupt vertical and lateral facies variations reflect syn-sedimentary faulting, coralline reef growth, and local variations in sediment supply (Said 1962). North- to northwest-trending faults were reactivated in late Oligocene to early Miocene time as west-dipping normal faults, resulting in tilting and emplacement of the platform sediment inlier blocks. Uplift and erosional truncation of fault blocks in the early Miocene culminated in development of a terminal erosion surface termed the mid-Tertiary pediplain. A second period of rift marginal uplift, active in post-Pliocene time has elevated the mid-Tertiary pediplain and exposed Quaternary wadi and reef terraces on the coastal plain (Purser and Philobbos 1993).

## 3. Sampling and methods

Twenty six sand samples (SF = 13, QS = 13) were collected from the lee side (upper, middle, lower third and end of dune ridge) of coastal dunes from the Red Sea coastal plain. Samples were not collected from the windward side of the dunes due to high disturbance caused by vegetation. Grain-size analysis of all samples was carried out in a Ro-Tap sieve shaker using American Society for Testing and Material (ASTM) sieves ranging from −1.5 to 4.25 φ at 0.50 φ intervals for 20 min (Folk 1966). Cumulative curves were constructed to calculate the statistical grain-size parameters (mean grain size and sorting values) by applying the equations of (Folk 1980) (table 1). Twenty six thin sections of bulk composition were prepared to examine the coastal dune sands. The point-counts were carried out using both Franzinelli and Potter (1983) and standard methods of 300 grains per thin section for the major compositional framework (quartz, feldspars and lithics, table 1). Heavy minerals were separated using bromoform (sp. gr. 2.85), and the composition of heavy minerals was counted under a binocular microscope for minor components like opaques (Op) (ironoxides) and non-opaque heavy minerals (NOp) (zircon, rutile, tourmaline, epidote, monazite, Mica (biotite, chlorite), hornblende, pyroxene, sphene, kyanite, biogenic shell and carbonates).

The 26 sand samples were dried at 110°C and treated with lithium metaborate and tetraborate to make pressed powder pellets. They were analyzed using X-ray fluorescence Pnalytical Axios Advanced XRF equipment for major and trace element geochemistry (Rollinson 1993). XRF analyses were performed at the laboratory of the Central Metallurgical Research and Development Institute, Egypt.

## 4. Results

### 4.1 *Texture and mineralogy*

Grain size parameters for the two investigated sites were calculated by applying the formula of Folk (1980) (table 1). The mean grain size (Mz) values show a homogenous trend in both SF (2.42–2.65 φ) and QS (2.04–2.59 φ) dune fields, which are fine sand size. Distinct differences in sorting ($\sigma$) are observed among the two investigated dune fields. The standard deviation (sorting) values of SF range from 0.38 to 0.41 φ, suggesting that SF sands are well sorted. However, the standard deviation values of QS vary from 0.53 φ (moderately well-sorted) to 1.0 φ (moderately sorted). Skewness ($Sk_i$) values of QS vary from 0.04 (near symmetrical) to –0.3 φ (coarse skewed), while a homogeneous trend is observed in SF sands, which are near symmetrical (0.02–0.07 φ). The kurtosis ($K_G$) values show a homogenous trend in both SF (0.95–1.0 φ) and QS (0.95–1.06 φ) dune fields, which are mesokurtic. The correlations between the mean grain size (Mz) and other textural parameters (sorting ($\sigma$); skewness ($Sk_i$) and kurtosis ($K_G$)) for the Red Sea coastal dune sands show two significant correlations between grain size and sorting, and grain size and skewness

Table 1. *Grain size, grain-size parameters and petrography of the coastal sand dunes of Red Sea, Egypt, expressed in %.*

| | Safaga | | | | | | | | | | | | | | |
|---|---|---|---|---|---|---|---|---|---|---|---|---|---|---|---|
| Location | SF1 | SF2 | SF3 | SF4 | SF5 | SF6 | SF7 | SF8 | SF9 | SF10 | SF11 | SF12 | SF13 | Av. | Std |
| Grain size% | | | | | | | | | | | | | | | |
| Sand | 87.8 | 91.3 | 89.5 | 80.5 | 76.9 | 89.3 | 92 | 91.3 | 89.8 | 86.8 | 82.5 | 91.9 | 90.3 | 87.7 | 4.8 |
| Mud | 1.1 | 0.9 | 0.7 | 0.5 | 1.3 | 1.5 | 1.3 | 1.4 | 1.8 | 1.8 | 1.3 | 0.7 | 0.8 | 1.2 | 0.4 |
| Carb. | 11.1 | 7.8 | 9.8 | 19 | 21.8 | 9.2 | 6.7 | 7.3 | 8.4 | 11.4 | 16.2 | 7.4 | 8.9 | 11.2 | 4.8 |
| Mz(ø) | 2.6 | 2.53 | 2.56 | 2.57 | 2.5 | 2.53 | 2.47 | 2.42 | 2.44 | 2.65 | 2.63 | 2.61 | 2.63 | 2.5 | 0.1 |
| $\sigma$(ø) | 0.4 | 0.39 | 0.38 | 0.38 | 0.39 | 0.38 | 0.39 | 0.39 | 0.39 | 0.39 | 0.39 | 0.38 | 0.41 | 0.4 | 0.0 |
| Ski | 0.07 | 0.05 | 0.06 | 0.06 | 0.03 | 0.03 | 0.03 | 0.02 | 0.03 | 0.05 | 0.04 | 0.05 | 0.04 | 0.04 | 0.0 |
| $K_G$ | 1 | 0.99 | 0.98 | 0.99 | 0.99 | 0.97 | 0.97 | 0.95 | 0.97 | 1 | 0.98 | 0.98 | 1 | 1.0 | 0.0 |
| Light fraction | | | | | | | | | | | | | | | |
| Qm% | 77.6 | 76.8 | 80.4 | 84 | 79.6 | 80.4 | 85.6 | 76 | 79.2 | 80 | 78.4 | 85.2 | 80.4 | 80.3 | 3.0 |
| Qp% | 0.8 | 2 | 0.8 | 1.6 | 1.6 | 0.8 | 0 | 1.6 | 1.2 | 1.2 | 1.2 | 1.2 | 0.4 | 1.1 | 0.5 |
| Qt% | 78.4 | 78.8 | 81.2 | 85.6 | 81.2 | 81.2 | 85.6 | 77.6 | 80.4 | 81.2 | 79.6 | 86.4 | 80.8 | 81.4 | 2.8 |
| Ft% | 8.8 | 10.4 | 10.8 | 6 | 8.8 | 6.8 | 9.2 | 8.8 | 9.2 | 7.6 | 6 | 6.8 | 8.4 | 8.3 | 1.5 |
| Lf% | 12.8 | 10.8 | 8 | 8.4 | 10 | 12 | 5.2 | 13.6 | 10.4 | 11.2 | 14.4 | 6.8 | 10.8 | 10.3 | 2.7 |
| | Quseir | | | | | | | | | | | | | | |
| | QS1 | QS2 | QS3 | QS4 | QS5 | QS6 | QS7 | QS8 | QS9 | QS10 | QS11 | QS12 | QS13 | Av. | Std |
| Grain size% | | | | | | | | | | | | | | | |
| Sand | 73.4 | 69.5 | 63.9 | 56.9 | 62.4 | 62.4 | 70.2 | 63.7 | 70.7 | 73 | 70 | 68.1 | 61.6 | 66.6 | 5.1 |
| Mud | 0.5 | 0.7 | 0.6 | 0.5 | 0.8 | 0.9 | 1.1 | 0.9 | 0.8 | 0.6 | 0.8 | 0.7 | 0.6 | 0.7 | 0.2 |
| Carb. | 26.1 | 29.8 | 35.5 | 42.6 | 36.8 | 36.7 | 28.7 | 35.4 | 28.5 | 26.4 | 29.2 | 31.2 | 37.8 | 31.6 | 5.6 |
| Mz(ø) | 2.49 | 2.54 | 2.41 | 2.6 | 2.6 | 2.59 | 2.59 | 2.1 | 2.45 | 2.04 | 2.4 | 2.5 | 2.59 | 2.5 | 0.2 |
| $\sigma$(ø) | 0.53 | 0.56 | 0.53 | 0.59 | 0.54 | 0.59 | 0.58 | 0.9 | 0.54 | 1 | 0.64 | 0.67 | 0.62 | 0.6 | 0.1 |
| Ski | −0.04 | −0.02 | −0.1 | 0.04 | 0.01 | 0.03 | 0.03 | −0.25 | −0.2 | −0.29 | −0.3 | −0.1 | −0.03 | −0.04 | 0.1 |
| $K_G$ | 1.03 | 1.01 | 1.04 | 0.98 | 0.98 | 0.97 | 0.96 | 0.99 | 1.06 | 0.95 | 1.02 | 1.01 | 1 | 1.0 | 0.0 |
| Light fraction | | | | | | | | | | | | | | | |
| Qm% | 78 | 84.8 | 79.2 | 77.6 | 86 | 85.2 | 76 | 76 | 79.6 | 75.6 | 76.8 | 78 | 78.8 | 79.4 | 3.6 |
| Qp% | 2 | 0.8 | 1.6 | 1.6 | 1.6 | 1.2 | 0.7 | 2.8 | 2.4 | 3.2 | 2.4 | 3.6 | 3.6 | 2.1 | 1.0 |
| Qt% | 80 | 85.6 | 80.8 | 79.2 | 87.6 | 86.4 | 76.7 | 78.8 | 82 | 78.8 | 79.2 | 81.6 | 82.4 | 81.5 | 3.3 |
| Ft% | 7.2 | 9.2 | 9.2 | 8 | 6.4 | 4.8 | 8.4 | 10.8 | 6.8 | 10.4 | 8.4 | 8.8 | 8.4 | 8.2 | 1.6 |
| Lf% | 12.8 | 5.2 | 10 | 12.8 | 6 | 8.8 | 14.9 | 10.4 | 11.2 | 10.8 | 12.4 | 9.6 | 9.2 | 10.3 | 2.7 |

Carb = carbonate; Mz = mean grain size (in f units); $\sigma$ = standard deviation (in f units); Ski = skewness; $K_G$ = kurtosis; Qm = monocrystalline quartz; Qp = polycrystalline quartz; Qt = total quartz; Ft = total feldspars; Lf = lithic fragment; Av. = average; Std = standard deviation.

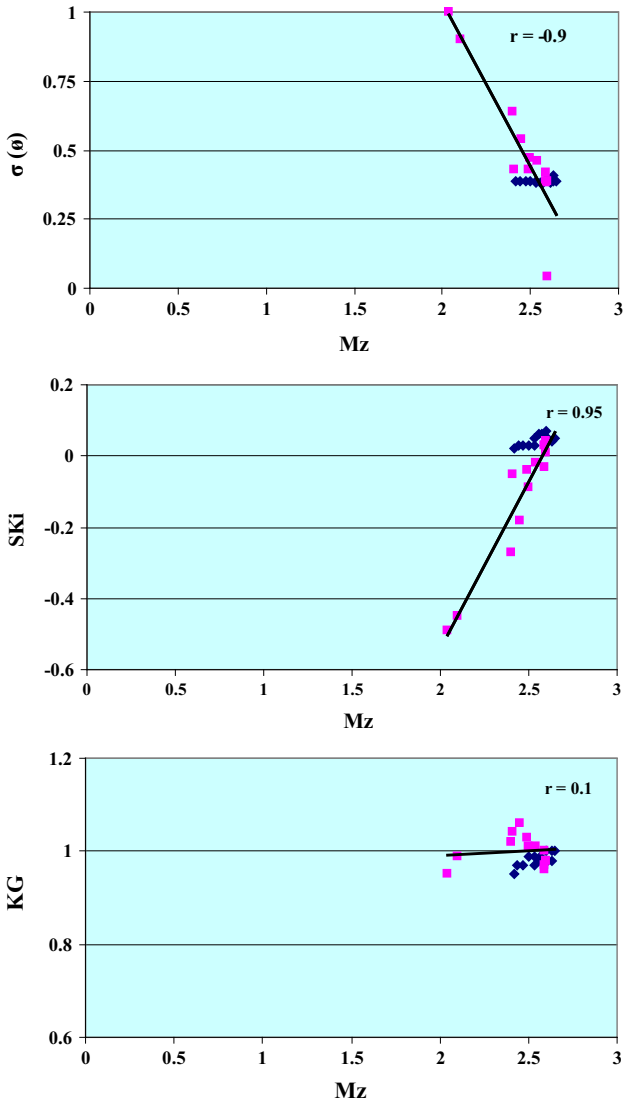


Figure 2. Binary diagrams of grain size (Mz) *vs.* sorting ($\sigma$), skewness (Ski) and kurtosis ($K_G$). Values ($r$) are the Pearson correlation coefficients that assess the degree to which two variables are related.

(Mansour and Sediek 1994; Mansour *et al.* 2000) (figure 2).

In the two studied fields, the coastal dune sands consist of quartz (monocrystalline (Qm) and polycrystalline (Qp)), feldspars (F) and lithic fragments (Lf). The Qt–Ft–Lt ternary diagrams (figure 3a; table 1) show that the examined sands of SF ($Qt_{81.4}$:$Ft_{8.3}$:$LF_{10.3}$) and QS ($Qt_{81.5}$:$Ft_{8.2}$:$LF_{10.3}$) are quartzosublithic sands. The abundance of quartz in both sites along the Red Sea coast is probably due to the maturity process, and indicates a recycled source.

The QmFLt ternary diagram (Dickinson *et al.* 1983) shows that the Red Sea coastal dune sands plot mainly in the recycled orogen field and partly in craton interior field (figure 3b). However, the composition of sands may reflect significant differences between SF and QS fields, supported by the average values and position of sand grains-mud matrix-carbonate cement (table 1). The southern area (QS) has carbonate (porcelanous foraminifera) content (31.6%) relatively higher than in the northern area (SF) sediments (av. 11.2%, table 1). The content is also relatively higher in the samples of the middle part of dune ridges than in the other parts (table 1).

Coastal dune sands are mainly composed of quartz (76.7–87.6%) and feldspar grains (4.8–10.8%, table 1). They constitute more than 80% of the sediments. However, the amount of biogenic fragments and shells, mostly soritides exceeds in the dunes at Quseir area. Quartz grains are fine, subrounded to well-rounded and moderately well-sorted. They are mostly monocrystalline with few polycrystalline. It contains tourmaline and apatite inclusions. Monocrystalline quartz grains are either uniform or undulatory extinction. Feldspars and rock fragments are also common in coastal dune sands. Lithic fragments consist mainly of sedimentary with metamorphic and plutonic fragments. Sedimentary rock fragments are carbonates, sandstone, siltstones and chert. Metamorphic fragments observed were probably gneisses. Plutonic lithics (i.e., granite and granodiorite) were observed.

The identified heavy minerals in the two studied dune fields are represented by non-opaque and opaque minerals (figure 4). Opaques such as magnetite, ilmenite, hematite and amorphous iron oxides are present (17.6–36.3%). The frequency percentage of heavy minerals is higher in the southern field (QS) and in samples of the upper part of the dunes (table 1). The lowest heavy mineral content is obtained from samples at the end (lower part) of dune ridges. However, no variation is noticed in the heavy mineral association of the two studied coastal dune fields. The most common minerals are the non-opaque minerals (63.7–82.4%) of total heavy minerals (table 2). They are more abundant in the dunes of QS sands.

Amphibole (green and brown hornblendes with minor riebeckite) is the most abundant non-opaque heavy minerals, averaging 40.9 and 53.7% in SF and QS coastal dune sands respectively. The grains are mostly prismatic in shape, however subrounded grains are also observed. The brown biotite is abundant, especially in SF (avg. 20.4%). Pyroxenes include both orthopyroxenes and clinopyroxenes. They are relatively abundant

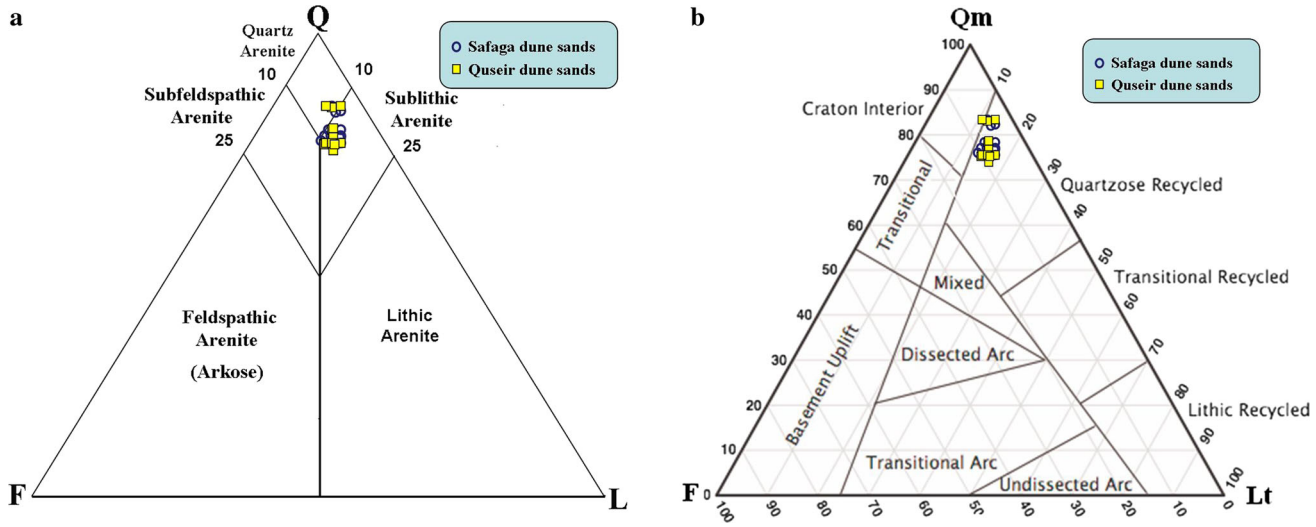


Figure 3. (**a**) QFL triangular diagram shows the classification of the coastal dune sands, modified after Dott (1964) and McBride (1963) and (**b**) QmFLt ternary diagram for the coastal dune sands after Dickinson *et al.* (1983).

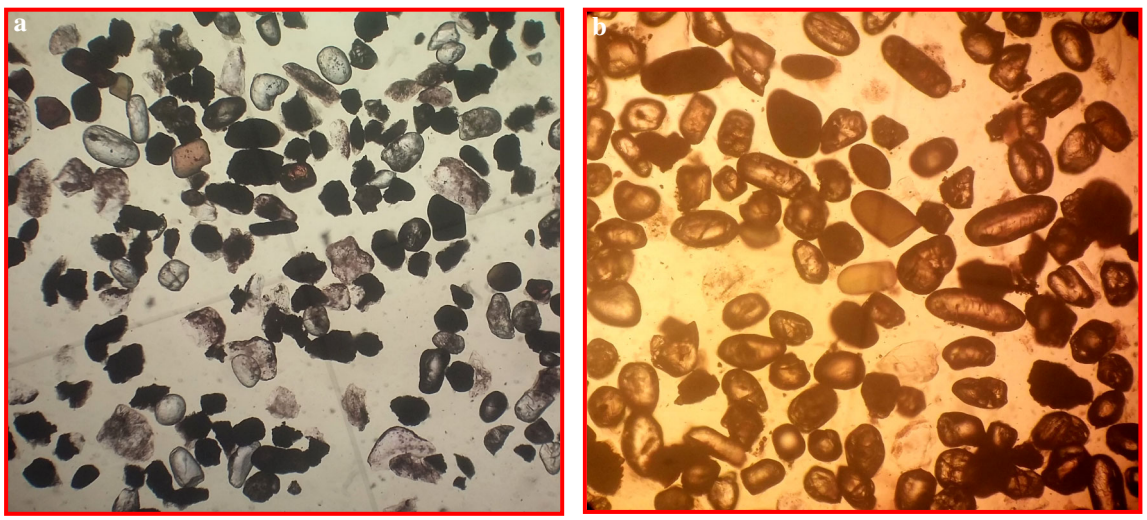


Figure 4. Photomicrograph of heavy minerals in coastal dune sand showing, opaques and non-opaques with different grain habits at (**a**) Safaga and (**b**) Quseir dune fields.

especially in QS (avg. 9.9%). Epidotes and monazites average 10.4 and 12.8% respectively are common in the dune SF sands. Chlorite and anhydrite (av. 5.7 and 5.0%, respectively) are relatively less abundant especially in QS sands. The ultrastable minerals (zircon, rutile and tourmaline) are very rare along the Red Sea coast (table 2). Other minerals include garnet staurolite, sphene, kyanite, andalusite, sillimanite and glauconite.

In SF, abundance of green hornblende, biotite, monazite, epidote and pyroxenes and scarcity of other minerals are characteristic of the dune field. Here andalusite and staurolite have highly concentration than QS coastal dune sands. The heavy mineral grains are subrounded to well-rounded as an indication of the long transportation distance from the hinterland Precambrian basement and Miocene and post-Miocene sedimentary rocks. The source rocks of sediments in the SF dune field are mainly derived from recycled older sedimentary with high effect of metamorphic-plutonic sources (Philobbos *et al.* 1983).

In QS, abundance of green and brown hornblende, pyroxenes, epidote and chlorite, and scarcity of other minerals are the most distinctive features of the dune field. However, sillimanite reaches its high content in the QS coastal dune sands. The heavy mineral grains are rounded as an indication

Table 2. *Distribution of heavy minerals in the coastal dune sands along the Red Sea, Egypt.*

| | Safaga | | | | | | | | | | | | | | |
|---|---|---|---|---|---|---|---|---|---|---|---|---|---|---|---|
| Location | SF1 | SF2 | SF3 | SF4 | SF5 | SF6 | SF7 | SF8 | SF9 | SF10 | SF11 | SF12 | SF13 | Av. | Std |
| Mineral | | | | | | | | | | | | | | | |
| Op | 59 | 43 | 43.5 | 26.5 | 41.8 | 39.2 | 27.2 | 22.3 | 29.1 | 42.6 | 41.5 | 31.6 | 24.4 | 36.3 | 10.4 |
| NOp | 41 | 57 | 56.5 | 73.5 | 58.2 | 60.8 | 72.8 | 77.7 | 70.9 | 57.4 | 58.5 | 68.4 | 75.6 | 63.7 | 10.4 |
| Non-opaques | | | | | | | | | | | | | | | |
| Zircon | 0.69 | 4.2 | 1.15 | 0.7 | 0.3 | 0 | 1.4 | 1.3 | 0 | 0 | 0.8 | 4.7 | 1.0 | 1.2 | 1.5 |
| Rutile | 0 | 1.5 | 2.1 | 0 | 0 | 1.55 | 0 | 0.4 | 0.65 | 0 | 0.8 | 1.0 | 0.7 | 0.7 | 0.7 |
| Tourmaline | 0.71 | 0.6 | 0 | 0.3 | 0.5 | 1.25 | 0.45 | 0.3 | 0 | 0.45 | 0.5 | 0.6 | 0.3 | 0.5 | 0.3 |
| Epidote | 25.3 | 17.8 | 8.55 | 10.9 | 9.3 | 12.2 | 12.4 | 11.9 | 3.35 | 3.3 | 14.5 | 11.9 | 10.4 | 11.7 | 5.7 |
| Monazite | 25.9 | 23.8 | 8.87 | 4.2 | 11.8 | 16.9 | 11.8 | 10.5 | 8.27 | 10.3 | 15.5 | 13.3 | 10.8 | 13.2 | 6.1 |
| Biotite | 5.6 | 12.7 | 12.2 | 30.1 | 31.7 | 15.5 | 18.9 | 23.3 | 34.2 | 21 | 16.5 | 20.1 | 20.9 | 20.2 | 8.2 |
| Chlorite | 1.4 | 0 | 1.63 | 1.3 | 0.75 | 0.55 | 0.92 | 7.4 | 4.53 | 7.95 | 1.3 | 0.7 | 1.1 | 2.3 | 2.6 |
| Hornblende | 30 | 26.7 | 50.1 | 46.6 | 37.5 | 37.6 | 44.7 | 40.6 | 46.6 | 50.1 | 39.7 | 36.8 | 44.2 | 40.9 | 7.2 |
| Pyroxene | 5.5 | 9.2 | 5.9 | 3.26 | 3.8 | 6.8 | 6.8 | 0 | 1.2 | 3.3 | 5.1 | 6.6 | 5.5 | 4.8 | 2.5 |
| Sphene | 1.4 | 2.2 | 1.5 | 0.9 | 1.85 | 0.55 | 0 | 0.9 | 0 | 0 | 1.7 | 1.2 | 1.1 | 1.0 | 0.7 |
| Kyanite | 0 | 0.7 | 0 | 0 | 0 | 0 | 0 | 0 | 0.6 | 2.3 | 0.0 | 0.3 | 0.0 | 0.3 | 0.6 |
| Andalusite | 0.7 | 0 | 5.9 | 1.3 | 2 | 3.5 | 1.3 | 0 | 0 | 0.9 | 3.0 | 1.7 | 3.1 | 1.8 | 1.7 |
| Staurolite | 0 | 0 | 0.8 | 0 | 0.5 | 3.6 | 0.8 | 0 | 0.6 | 0 | 0.4 | 1.2 | 0.7 | 0.7 | 1.0 |
| Sillimanite | 0.7 | 0 | 0 | 0 | 0 | 0 | 0.5 | 0.9 | 0 | 0.5 | 0.3 | 0.0 | 0.2 | 0.2 | 0.3 |
| Garnet | 0 | 0 | 0 | 0 | 0 | 0 | 0 | 0 | 0 | 0 | 0.0 | 0.0 | 0.0 | 0.0 | 0.0 |
| Glauconite | 0 | 0 | 0 | 0 | 0 | 0 | 0 | 0 | 0 | 0 | 0.0 | 0.0 | 0.0 | 0.0 | 0.0 |
| Anhydrite | 2.1 | 0.7 | 1.3 | 0.44 | 0 | 0 | 0 | 2.6 | 0 | 0 | 0.0 | 0.0 | 0.0 | 0.5 | 0.9 |
| Op/NOp | 1.44 | 0.75 | 0.77 | 0.36 | 0.72 | 0.64 | 0.37 | 0.29 | 0.41 | 0.74 | 0.71 | 0.46 | 0.32 | 0.6 | 0.3 |
| ZRT | 1.4 | 6.3 | 3.25 | 1 | 0.8 | 2.8 | 1.85 | 2 | 0.65 | 0.45 | 2.05 | 6.30 | 1.97 | 2.4 | 1.9 |
| ZRT/PH | 0.04 | 0.18 | 0.06 | 0.02 | 0.02 | 0.06 | 0.04 | 0.05 | 0.01 | 0.01 | 0.05 | 0.15 | 0.04 | 0.1 | 0.1 |
| EG/PHZRT | 0.69 | 0.42 | 0.14 | 0.21 | 0.22 | 0.26 | 0.23 | 0.28 | 0.07 | 0.06 | 0.31 | 0.24 | 0.2 | 0.3 | 0.2 |
| MF | 35.5 | 35.9 | 56 | 49.9 | 41.3 | 44.4 | 51.5 | 40.6 | 47.8 | 53.4 | 44.8 | 43.4 | 49.7 | 45.7 | 6.4 |
| MT | 55.3 | 44.5 | 58.7 | 57.5 | 46.8 | 49.8 | 57.1 | 52.5 | 50 | 53.4 | 54.2 | 48.7 | 54.6 | 52.5 | 4.3 |
| GM | 28.7 | 29.3 | 16.7 | 6.5 | 15.1 | 25.3 | 16.3 | 13 | 9.47 | 14.4 | 20.5 | 21.8 | 16.1 | 17.9 | 6.9 |

Table 2. *(Continued.)*

| Location | Quseir | | | | | | | | | | | | | | |
|---|---|---|---|---|---|---|---|---|---|---|---|---|---|---|---|
| | QS1 | QS2 | QS3 | QS4 | QS5 | QS6 | QS7 | QS8 | QS9 | QS10 | QS11 | QS12 | QS13 | Av. | Std |
| Mineral | | | | | | | | | | | | | | | |
| Op | 18.5 | 21 | 8.9 | 16.3 | 11.3 | 37.9 | 11.1 | 9.9 | 26.1 | 10.8 | 21.4 | 16.2 | 19.5 | 17.6 | 8.1 |
| NOp | 81.5 | 79 | 91.1 | 83.7 | 88.7 | 62.1 | 88.9 | 90.1 | 73.9 | 89.2 | 78.6 | 83.8 | 80.5 | 82.4 | 8.1 |
| Non-opaques | | | | | | | | | | | | | | | |
| Zircon | 1.1 | 2.1 | 0.6 | 1.5 | 1.2 | 0.6 | 0 | 0.65 | 0.85 | 1.8 | 0.9 | 1.05 | 0.6 | 1.0 | 0.6 |
| Rutile | 0 | 0 | 0 | 0 | 0 | 0 | 0 | 0 | 0 | 0 | 0 | 0 | 0 | 0.0 | 0.0 |
| Tourmaline | 0 | 0 | 0.6 | 0 | 0 | 0 | 0 | 0.6 | 0.3 | 0 | 0.3 | 0 | 0 | 0.1 | 0.2 |
| Epidote | 8.3 | 9.5 | 8.5 | 9.7 | 11.4 | 11.6 | 1.55 | 8.8 | 8.4 | 9.6 | 9.95 | 10.7 | 6.48 | 8.8 | 2.6 |
| Monazite | 0 | 0 | 0 | 0 | 0 | 0 | 0 | 0.6 | 0 | 0 | 0 | 0 | 0 | 0.0 | 0.2 |
| Biotite | 1.4 | 7.4 | 6.5 | 6.3 | 3.65 | 0 | 5.9 | 6.1 | 3.95 | 6.85 | 5.08 | 3.15 | 4.78 | 4.7 | 2.2 |
| Chlorite | 6.6 | 4.2 | 7.5 | 7.8 | 0 | 7.8 | 7.4 | 4.8 | 7.05 | 6 | 3.75 | 7.8 | 3.7 | 5.7 | 2.3 |
| Hornblende | 53.4 | 45.7 | 49.7 | 44.7 | 56.1 | 55.6 | 74.2 | 53.4 | 51.55 | 45.2 | 52.9 | 50.2 | 65.2 | 53.7 | 8.2 |
| Pyroxene | 12.8 | 9.6 | 9.8 | 9.3 | 13.4 | 10.8 | 5.4 | 5.9 | 11.3 | 9.45 | 11.6 | 10.1 | 9.4 | 9.9 | 2.3 |
| Sphene | 0.5 | 0 | 0 | 0 | 0 | 0 | 0 | 0 | 0.25 | 0 | 0 | 0 | 0 | 0.1 | 0.1 |
| Kyanite | 0 | 0 | 0 | 0.6 | 0.6 | 0 | 0 | 4.5 | 0 | 0.3 | 0.3 | 0.3 | 0.3 | 0.5 | 1.2 |
| Andalusite | 3.9 | 3.3 | 2.9 | 2.1 | 4.1 | 9.3 | 3.3 | 3.9 | 3.4 | 2.7 | 3.5 | 5.7 | 3.7 | 4.0 | 1.8 |
| Staurolite | 0 | 0 | 0 | 0 | 2.8 | 0 | 0.6 | 0 | 0 | 0 | 1.4 | 0 | 1.7 | 0.5 | 0.9 |
| Sillimanite | 4.3 | 3.2 | 0.8 | 2.6 | 2.2 | 2.2 | 0.6 | 0 | 2.55 | 2.9 | 1.5 | 2.4 | 1.4 | 2.1 | 1.2 |
| Garnet | 0 | 2.1 | 0 | 0 | 2.8 | 0 | 0 | 0 | 0 | 1.05 | 1.4 | 0 | 1.4 | 0.7 | 1.0 |
| Glauconite | 0 | 6.4 | 5.7 | 7.8 | 0 | 0 | 0 | 4.65 | 2.85 | 7.1 | 2.85 | 3.9 | 0 | 3.2 | 3.0 |
| Anhydrite | 7.7 | 6.5 | 7.4 | 7.6 | 1.75 | 2.1 | 1.05 | 6.1 | 7.55 | 7.05 | 4.58 | 4.85 | 1.4 | 5.0 | 2.6 |
| Op/NOp | 0.3 | 0.27 | 0.1 | 0.19 | 0.13 | 0.61 | 0.12 | 0.11 | 0.353 | 0.121 | 0.272 | 0.193 | 0.242 | 0.2 | 0.1 |
| ZRT | 1.9 | 2.1 | 1.2 | 1.5 | 1.2 | 0.6 | 0 | 1.25 | 1.15 | 1.8 | 1.2 | 1.05 | 0.6 | 1.1 | 0.5 |
| ZRT/PH | 0.1 | 0.04 | 0.02 | 0.03 | 0.02 | 0.01 | 0.00 | 0.02 | 0.02 | 0.03 | 0.02 | 0.02 | 0.01 | 0.0 | 0.0 |
| EG/PHZRT | 0.2 | 0.2 | 0.14 | 0.17 | 0.2 | 0.17 | 0.02 | 0.15 | 0.131 | 0.189 | 0.173 | 0.174 | 0.105 | 0.2 | 0.0 |
| MF | 6.4 | 55.3 | 59.5 | 54 | 69.5 | 66.4 | 79.6 | 59.3 | 62.85 | 54.65 | 64.5 | 60.2 | 74.55 | 63.6 | 7.7 |
| MT | 4.3 | 57.3 | 58.2 | 54.4 | 70.3 | 67.2 | 75.8 | 62.2 | 59.95 | 55.85 | 64.25 | 60.8 | 73.03 | 63.1 | 6.7 |
| GM | 6.9 | 8.6 | 4.9 | 6.8 | 10.9 | 12.1 | 4.5 | 10.3 | 7.1 | 7.7 | 7.9 | 9.45 | 7.7 | 8.2 | 2.2 |

Av. = average; Std = standard deviation; Op = opaques; NOp = non-opaques; ZRT = zircon + rutile + tourmaline; PH = pyroxene + hornblende (amphiboles); EG = epidote + garnet; MF (common constituents of mafic magmatic rocks) = total content of all pyroxene, brown-green hornblende and olivine; MT (common constituents of basic metamorphic rocks) = total content of pale colored and blue green amphiboles, epidote (group) and garnet; GM (accessory minerals of granites and sialic metamorphic rocks) = total content of zircon, tourmaline, staurolite, kyanite, andalusite, monazite and sillimanite.

of long transportation distance from the hinterland older rocks. The source rocks of sediments in the QS dune field are mainly derived from Miocene and post-Miocene rocks with low effect of Precambrian metavolcanic, metagabbro, and granite (Dar 1998).

### 4.2 *Major element geochemistry*

The XRF analyses of whole-rock coastal dune sands of Safaga (SF) and Quseir (QS) are given in table 3. The provenance discriminant function diagram of Roser and Korsch (1988), (figure 5) shows that there are two major provinces, which influence the composition of coastal dune sands: the quartzose and felsic provinces being the SF coastal dune sands located mainly in quartzose sedimentary provinces except six sample plots in the felsic igneous provinces, whereas the QS coastal dune sands placed exclusively in the quartzose sedimentary provinces.

In the A–B–C and $CaO–Na_2O–K_2O$ ternary diagrams (Kasper-Zubillaga and Zolezzi-Ruiz 2007) show that the coastal dune sands for both SF and QS plot exclusively in the coastal dune field (figure 6a, b), which can be attributed to the compositional maturity near the coast. This can be indicated by the high silica and low feldspar and rock fragments for both the studied coastal dune fields.

### 4.3 *Trace element geochemistry*

The results of trace element concentrations for the two investigated sites are given in table 4. The average upper continental crust (UCC) normalized data (Taylor and McLennan 1985) of trace elements shows higher concentration of Sr, Ba, Co, Cr, Zr, Y, Nb, and Rb and depletion of V, Ni, Zn, Cu and Pb for coastal dune sands at the two studied dune fields (figure 7). However, there are slight differences in trace element contents among the two investigated dune fields, which may be the result from the sorting effect of sands or differences in source rock compositions.

The high enrichment in Sr content in coastal dunes (table 4) and the positive correlation between Sr and CaO ($r = 0.769$), indicate their original concentrations in the skeleton of marine organisms. SF and QS coastal dune sands contain high concentration of large ion lithophile elements such as Rb and Ba. In addition, Rb and Ba show positive correlation with $K_2O$ ($r = 0.788$; 0.603, respectively) for both the coastal dune sands, reflecting that these mineral distribution controlled by alkali feldspar (Armstrong-Altrin *et al.* 2015a; Zaid 2015c). Zr content in SF coastal dune sands ($70 \pm 10$, $n = 13$) is higher than that in QS sands ($16 \pm 4$, $n = 13$). The correlation between Zr and $Fe_2O_3$ ($r = 0.939$) are well correlated for SF and QS sands, suggesting that this element may be hosted by zircon and/or magnetite. The transitional elements like Cr and Cu are more concentrated in SF than QS coastal dune sands. In addition, Cr and Cu show positive correlation with $Al_2O_3$ ($r = 0.669$; 0.65, respectively) for both the sands, indicating that these transitional elements are mainly associated with clay minerals. The presence of Y in both the studied coastal dune fields, indicate basaltic and metamorphic sources (Hill *et al.* 2000).

## 5. Discussion

### 5.1 *Texture parameters and modal analysis*

The negative correlation between Mz(ø) and σ(ø) for the Red Sea coastal dune sands (figure 2a) reflect a wide coastal plain for both SF and QS dune fields, which allows a deposition of various terrigenous sand sizes. In addition, the mean grain size values are dispersed with the presence of shell fragments (Wang *et al.* 2003). The positive correlation between Mz(ø) and Ski(ø) for both SF and QS coastal dune sands (figure 2b) may be due to long-shore processes along the coastal plain close to river mouth discharging coarse sediments. The linear relationship between Mz(ø) and $K_G$(ø) suggest that the sands of both SF and QS dune fields (figure 2c) are affected by onshore winds and long-shore currents which pick up and transport sand grains and shell detritus into a wide Red Sea coastal plain at the border of the beach producing mesokurtic curves.

The SF coastal dune sands seem to have the similar mineralogical composition as the QS coastal dune sands (figure 3a). The mineralogical component Qt–Ft–Lt, indicates that SF and QS coastal dune sands are affected by quartz-rich sands. The abundance of quartz within dune sands may be due to the continuous supply of sedimentary rock fragments that are composed mainly of sandstone and shales into dune fields. The presence of sedimentary lithic fragments besides metamorphic-plutonic lithics in both SF and QS coastal dune sands indicated that these dune sands were influenced by alluvial sands from adjacent wadis. The recorded

Table 3. *Major element concentrations (wt%) in fine fraction of the coastal dune sands along Red Sea, Egypt.*

| | Safaga | | | | | | | | | | | | | | |
|---|---|---|---|---|---|---|---|---|---|---|---|---|---|---|---|
| Location | SF1 | SF2 | SF3 | SF4 | SF5 | SF6 | SF7 | SF8 | SF9 | SF10 | SF11 | SF12 | SF13 | Av. | Std |
| $(SiO_2)_{adj}$ | 79.68 | 81.27 | 80.64 | 79.53 | 78.95 | 80.28 | 82.12 | 81.08 | 80.42 | 78.94 | 79.70 | 81.11 | 80.09 | 80.29 | 0.95 |
| $SiO_2$ | 78.29 | 80.4 | 79.7 | 77.89 | 76.51 | 79.08 | 80.79 | 80.19 | 79.1 | 78 | 78.03 | 80 | 78.66 | 78.97 | 1.23 |
| $TiO_2$ | 0.85 | 0.52 | 0.6 | 1.2 | 1.45 | 0.74 | 0.47 | 0.54 | 0.58 | 1.02 | 1.08 | 0.44 | 0.51 | 0.77 | 0.32 |
| $Al_2O_3$ | 9.4 | 8.9 | 8.9 | 9.4 | 9.6 | 9.6 | 8.7 | 9.4 | 9.2 | 9.9 | 9.9 | 9.5 | 9.6 | 9.38 | 0.37 |
| $Fe_2O_3^*$ | 1.8 | 1.7 | 1.72 | 1.9 | 1.89 | 1.75 | 1.73 | 1.69 | 1.72 | 1.84 | 1.89 | 1.73 | 1.71 | 1.77 | 0.08 |
| MnO | 0.03 | 0.04 | 0.05 | 0.04 | 0.03 | 0.04 | 0.04 | 0.05 | 0.05 | 0.04 | 0.04 | 0.05 | 0.04 | 0.04 | 0.01 |
| MgO | 0.32 | 0.39 | 0.28 | 0.4 | 0.37 | 0.27 | 0.34 | 0.39 | 0.28 | 0.34 | 0.4 | 0.34 | 0.39 | 0.35 | 0.05 |
| CaO | 4.3 | 3.6 | 4.2 | 4.11 | 4.1 | 3.8 | 2.9 | 3.35 | 4.2 | 4.3 | 3.2 | 3.3 | 4 | 3.80 | 0.48 |
| $Na_2O$ | 1.81 | 1.86 | 1.89 | 1.87 | 1.88 | 1.89 | 1.91 | 1.88 | 1.89 | 1.92 | 1.86 | 1.87 | 1.89 | 1.88 | 0.03 |
| $K_2O$ | 1.43 | 1.49 | 1.45 | 1.1 | 1.05 | 1.3 | 1.46 | 1.38 | 1.3 | 1.41 | 1.48 | 1.36 | 1.39 | 1.35 | 0.14 |
| $P_2O_5$ | 0.03 | 0.03 | 0.04 | 0.03 | 0.03 | 0.04 | 0.04 | 0.03 | 0.04 | 0.04 | 0.03 | 0.04 | 0.03 | 0.03 | 0.01 |
| LOI | 1.74 | 1.07 | 1.17 | 2.06 | 3.09 | 1.49 | 1.62 | 1.1 | 1.64 | 1.19 | 2.09 | 1.37 | 1.78 | 1.65 | 0.55 |
| Total | 100 | 100 | 100 | 100 | 100 | 100 | 100 | 100 | 100 | 100 | 100 | 100 | 100 | 100 | 0.00 |
| CaO* | 0.03 | 0.03 | 0.03 | 0.03 | 0.03 | 0.03 | 0.03 | 0.03 | 0.03 | 0.03 | 0.03 | 0.03 | 0.03 | 0.03 | 0.00 |
| CIA | 55.49 | 53.38 | 53.21 | 56.04 | 56.64 | 55.62 | 52.40 | 54.92 | 54.57 | 55.68 | 56.06 | 55.36 | 55.30 | 54.97 | 1.26 |
| ICV | 1.12 | 1.08 | 1.14 | 1.13 | 1.12 | 1.02 | 1.02 | 0.99 | 1.09 | 1.10 | 1.01 | 0.96 | 1.03 | 1.06 | 0.06 |
| $Al_2O_3/TiO_2$ | 11.06 | 17.12 | 14.83 | 7.83 | 6.62 | 12.97 | 18.51 | 17.41 | 15.86 | 9.71 | 9.17 | 21.59 | 18.82 | 13.96 | 4.75 |
| $K_2O/Na_2O$ | 0.79 | 0.80 | 0.77 | 0.59 | 0.56 | 0.69 | 0.76 | 0.73 | 0.69 | 0.73 | 0.80 | 0.73 | 0.74 | 0.72 | 0.08 |
| $SiO_2/Al_2O_3$ | 8.33 | 9.03 | 8.96 | 8.29 | 7.97 | 8.24 | 9.29 | 8.53 | 8.60 | 7.88 | 7.88 | 8.42 | 8.19 | 8.43 | 0.44 |

Table 3. *(Continued.)*

| Location | Quseir | | | | | | | | | | | | | | |
|---|---|---|---|---|---|---|---|---|---|---|---|---|---|---|---|
| | QS1 | QS2 | QS3 | QS4 | QS5 | QS6 | QS7 | QS8 | QS9 | QS10 | QS11 | QS12 | QS13 | Av. | Std |
| $(SiO_2)_{adj}$ | 75.98 | 75.12 | 76.13 | 77.66 | 76.13 | 75.45 | 76.74 | 77.32 | 76.15 | 77.41 | 76.80 | 76.39 | 77.45 | 76.52 | 0.79 |
| $SiO_2$ | 66.50 | 65.50 | 67.20 | 70.90 | 68.16 | 66.40 | 71.14 | 69.70 | 70.70 | 72.53 | 70.10 | 69.10 | 70.10 | 69.08 | 2.15 |
| $TiO_2$ | 1.56 | 1.46 | 1.33 | 1.16 | 1.29 | 1.30 | 1.48 | 1.33 | 1.49 | 1.54 | 1.45 | 1.41 | 1.26 | 1.39 | 0.12 |
| $Al_2O_3$ | 7.50 | 8.15 | 7.69 | 7.10 | 7.90 | 7.96 | 8.22 | 7.38 | 8.26 | 7.88 | 8.20 | 8.04 | 7.50 | 7.83 | 0.37 |
| $Fe_2O_3^*$ | 1.50 | 1.40 | 1.27 | 1.11 | 1.23 | 1.23 | 1.27 | 1.26 | 1.42 | 1.48 | 1.41 | 1.38 | 1.29 | 1.33 | 0.11 |
| MnO | 0.04 | 0.03 | 0.05 | 0.05 | 0.04 | 0.04 | 0.05 | 0.05 | 0.03 | 0.04 | 0.05 | 0.05 | 0.04 | 0.04 | 0.01 |
| MgO | 1.44 | 1.47 | 1.52 | 1.59 | 1.43 | 1.54 | 1.35 | 1.50 | 1.48 | 1.30 | 1.37 | 1.41 | 1.58 | 1.46 | 0.09 |
| CaO | 5.10 | 5.40 | 5.30 | 5.60 | 5.60 | 5.70 | 5.00 | 4.80 | 5.50 | 5.00 | 4.90 | 5.20 | 5.10 | 5.25 | 0.29 |
| $Na_2O$ | 2.10 | 1.98 | 2.15 | 1.99 | 2.09 | 2.04 | 2.15 | 2.31 | 1.94 | 1.95 | 1.86 | 1.87 | 1.81 | 2.02 | 0.14 |
| $K_2O$ | 1.75 | 1.76 | 1.73 | 1.77 | 1.75 | 1.75 | 2.00 | 1.78 | 1.99 | 1.94 | 1.91 | 1.96 | 1.79 | 1.84 | 0.10 |
| $P_2O_5$ | 0.03 | 0.04 | 0.03 | 0.03 | 0.04 | 0.04 | 0.04 | 0.03 | 0.03 | 0.04 | 0.03 | 0.04 | 0.04 | 0.04 | 0.01 |
| LOI | 12.48 | 12.81 | 11.73 | 8.70 | 10.47 | 12.00 | 7.30 | 9.86 | 7.16 | 6.30 | 8.72 | 9.54 | 9.49 | 9.74 | 2.11 |
| Total | 100.0 | 100.0 | 100.0 | 100.0 | 100.0 | 100.0 | 100.0 | 100.0 | 100.0 | 100.0 | 100.0 | 100.0 | 100.0 | 100.0 | 0.00 |
| CaO* | 0.03 | 0.03 | 0.03 | 0.03 | 0.03 | 0.03 | 0.03 | 0.04 | 0.03 | 0.03 | 0.03 | 0.03 | 0.03 | 0.03 | 0.00 |
| CIA | 45.87 | 49.05 | 46.10 | 45.48 | 47.26 | 47.92 | 46.94 | 43.53 | 49.02 | 47.91 | 49.89 | 49.13 | 48.57 | 47.44 | 1.81 |
| ICV | 1.80 | 1.66 | 1.74 | 1.87 | 1.70 | 1.71 | 1.62 | 1.77 | 1.68 | 1.68 | 1.58 | 1.65 | 1.72 | 1.70 | 0.08 |
| $Al_2O_3/TiO_2$ | 4.81 | 5.58 | 5.78 | 6.12 | 6.12 | 6.12 | 5.55 | 5.55 | 5.54 | 5.12 | 5.66 | 5.70 | 5.95 | 5.66 | 0.39 |
| $K_2O/Na_2O$ | 0.83 | 0.89 | 0.80 | 0.89 | 0.84 | 0.86 | 0.93 | 0.77 | 1.03 | 0.99 | 1.03 | 1.05 | 0.99 | 0.92 | 0.09 |
| $SiO_2/Al_2O_3$ | 8.87 | 8.04 | 8.74 | 9.99 | 8.63 | 8.34 | 8.65 | 9.44 | 8.56 | 9.20 | 8.55 | 8.59 | 9.35 | 8.84 | 0.52 |

$(SiO_2)$adj = major-element data were recalculated to anhydrous (LOI-free) basis and adjusted to 100%; $Fe_2O_3$* = Total Fe expressed as $Fe_2O_3$. CIA = $[Al_2O_3 / (Al_2O_3 + CaO^* + Na_2O + K_2O)] \times 100$ (Nesbitt and Young 1982). CaO* = CaO in silicate phase. To calculate CaO* the assumption proposed by McLennan *et al.* (1993) was followed. ICV = $(Fe_2O_3 + K_2O + Na_2O + CaO + MgO + MnO + TiO_2)/Al_2O_3$ (Cox *et al.* 1995).

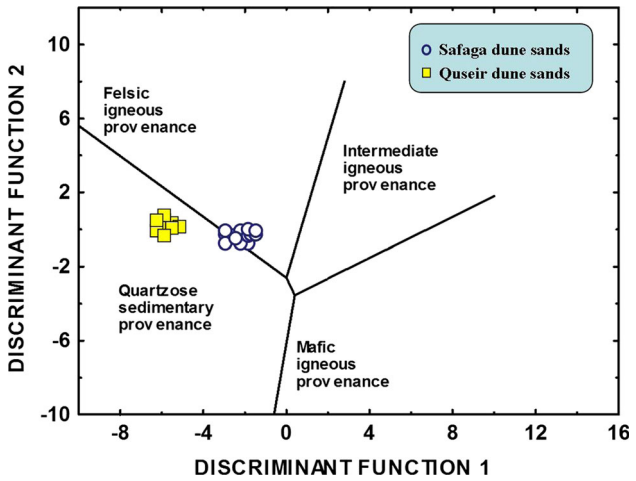


Figure 5. Major elements provenance discriminant function diagram for the coastal dune sands (Roser and Korsch 1988). The discriminant functions are: Discriminant Function 1 = $(-1.773 \cdot TiO_2) + (0.607 \cdot Al_2O_3) + (0.760 \cdot Fe_2O_3) + (-1.500 \cdot MgO) + (0.616 \cdot CaO) + (0.509 \cdot Na_2O) + (-1.224 \cdot K_2O) + (-9.090)$; Discriminant Function 2 = $(0.445 \cdot TiO_2) + (0.070 \cdot Al_2O_3) + (-0.250 \cdot Fe_2O_3) + (-1.142 \cdot MgO) + (0.438 \cdot CaO) + (1.475 \cdot Na_2O) + (1.426 \cdot K_2O) + (-6.861)$.

carbonate material in the light fraction proved its derivation from the beach zone where winds picked up and moved grains to form part of the sand dunes at the border of the beach.

### 5.2 *Weathering conditions and hydraulic sorting*

There are many weathering indices been developed and are extensively used to identify the chemical weathering intensity of the source area (Armstrong-Altrin 2015; Armstrong-Altrin *et al.* 2015a; Kassi *et al.* 2015; Zaid 2015c). Among these weathering indices, a chemical index of alteration (CIA; Nesbitt and Young 1982) is widely used to determine the degree of the source area weathering. The CIA values for the SF and QS coastal dune sands are ($54.97 \pm 1.26$, $n = 13$) and ($47.44 \pm 1.81$, $n = 13$) respectively (table 3) and are low relative to the range of the post-Archean Australian shale (PAAS) value (70–75; Taylor and McLennan 1985). However, the average CIA values in QS coastal dune sands is lower than in SF coastal dune sands, the differences in average CIA values among the two investigated dune fields are not statistically significant (Armstrong-Altrin 2009). These values suggest arid climate and a low intensity of chemical weathering.

The CIA values of SF and QS coastal dune sand samples are plotted in the ACNK diagram (figure 8). The degree of weathering is quite variable for both the studied sites. All samples are scattered around the feldspar join line (figure 8), which reveals steady state weathering conditions. These conditions occur where climate and tectonism vary greatly, altering the rates of chemical weathering and erosion, and resulting in the production of chemically diverse sediments (Armstrong-Altrin 2009). All samples are mostly scattered around the plagioclase – K-feldspar line near upper crust source (figure 8), suggesting recycled older sedimentary source rocks (Nesbitt and Young 1984). The smaller differences among the CIA values of SF and QS coastal dune sand samples also suggest a recycled older sedimentary source.

The calculated Rb/Sr ratio values (table 4) of the investigated SF ($0.1 \pm 0.01$) and QS ($0.06 \pm 0.04$)

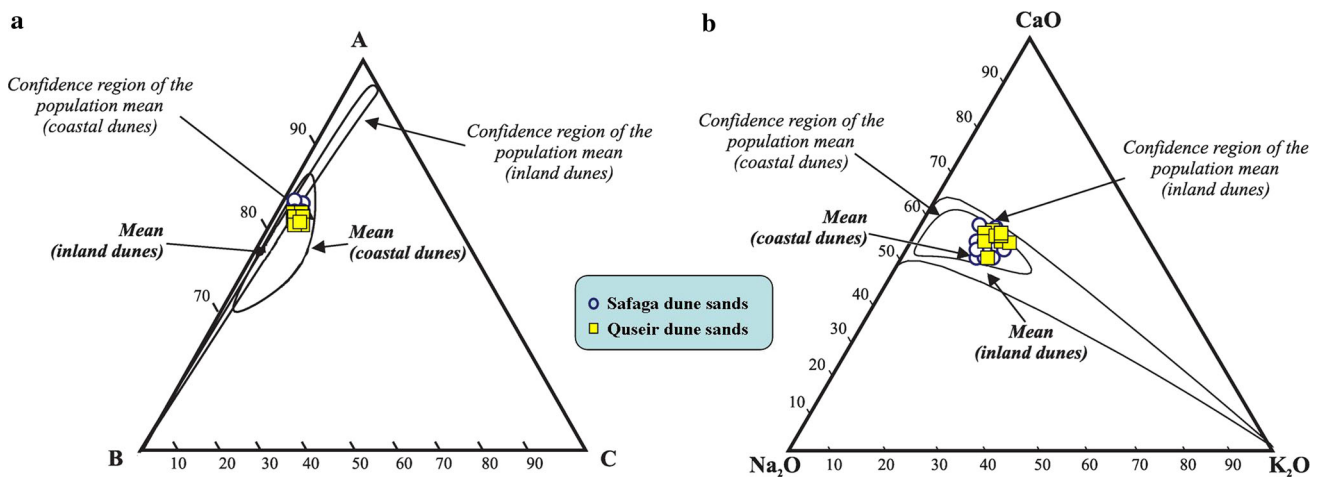


Figure 6. (**a**) A–B–C ternary diagram for the Eastern Desert coastal dune sands where A = $SiO_2$, B = $K_2O + Na_2O + Al_2O_3$ and C = $Fe_2O_3 + TiO_2 + MgO$ (after Kasper-Zubillaga and Zolezzi-Ruiz 2007). (**b**) CaO–$Na_2O$–$K_2O$ ternary diagram for the Eastern Desert coastal dune sands (after Kasper-Zubillaga and Zolezzi-Ruiz 2007).

Table 4. *Trace element concentrations (ppm) in coastal dune sands along Red Sea, Egypt.*

| | Safaga | | | | | | | | | | | | | | |
|---|---|---|---|---|---|---|---|---|---|---|---|---|---|---|---|
| Location | SF1 | SF2 | SF3 | SF4 | SF5 | SF6 | SF7 | SF8 | SF9 | SF10 | SF11 | SF12 | SF13 | Av. | Std |
| Sr | 415 | 332 | 373 | 461 | 387 | 392 | 319 | 325 | 366 | 436 | 427 | 309 | 349 | 376 | 49 |
| Rb | 39 | 38 | 43 | 36 | 35 | 41 | 36 | 37 | 42 | 41 | 38 | 35 | 40 | 39 | 3 |
| Ba | 505 | 404 | 454 | 561 | 380 | 476 | 388 | 396 | 445 | 530 | 502 | 376 | 424 | 449 | 61 |
| V | 11 | 9 | 15 | 7 | 8 | 16 | 17 | 14 | 15 | 11 | 11 | 12 | 14 | 12 | 3 |
| Ni | 9 | 8 | 12 | 6 | 7 | 13 | 13 | 11 | 11 | 9 | 8 | 10 | 10 | 10 | 2 |
| Co | 68 | 54 | 61 | 81 | 64 | 64 | 69 | 63 | 60 | 71 | 73 | 67 | 57 | 66 | 7 |
| Cr | 44 | 35 | 40 | 18 | 49 | 42 | 34 | 35 | 39 | 46 | 18 | 33 | 37 | 36 | 9 |
| Zn | 5 | 4 | 4 | 6 | 3 | 5 | 4 | 4 | 4 | 5 | 3 | 4 | 4 | 4 | 1 |
| Cu | 19 | 15 | 17 | 21 | 12 | 18 | 15 | 15 | 17 | 20 | 18 | 14 | 16 | 17 | 3 |
| Zr | 76 | 60 | 68 | 84 | 76 | 85 | 58 | 59 | 67 | 79 | 81 | 56 | 64 | 70 | 10 |
| Y | 21 | 17 | 9 | 15 | 16 | 10 | 16 | 16 | 9 | 12 | 22 | 16 | 18 | 15 | 4 |
| Pb | 6 | 4 | 3 | 7 | 6 | 3 | 3 | 4 | 3 | 5 | 6 | 3 | 4 | 4 | 1 |
| Nb | 21 | 17 | 19 | 23 | 19 | 20 | 16 | 16 | 18 | 22 | 27 | 15 | 17 | 19 | 3 |
| Rb/Sr | 0.09 | 0.11 | 0.11 | 0.08 | 0.09 | 0.10 | 0.11 | 0.11 | 0.11 | 0.09 | 0.09 | 0.11 | 0.11 | 0.10 | 0.01 |
| | Quseir | | | | | | | | | | | | | | |
| | QS1 | QS2 | QS3 | QS4 | QS5 | QS6 | QS7 | QS8 | QS9 | QS10 | QS11 | QS12 | QS13 | Av. | Std |
| Sr | 272 | 992 | 942 | 825 | 914 | 952 | 888 | 961 | 940 | 268 | 964 | 962 | 878 | 828 | 251 |
| Rb | 36 | 41 | 43 | 46 | 42 | 43 | 40 | 34 | 41 | 39 | 41 | 42 | 43 | 41 | 3 |
| Ba | 599 | 437 | 415 | 363 | 403 | 419 | 474 | 423 | 456 | 594 | 451 | 406 | 387 | 448 | 72 |
| V | 16 | 13 | 14 | 15 | 13 | 14 | 15 | 14 | 14 | 24 | 14 | 13 | 14 | 15 | 3 |
| Ni | 14 | 12 | 13 | 13 | 12 | 13 | 14 | 13 | 13 | 23 | 22 | 12 | 13 | 14 | 4 |
| Co | 65 | 67 | 69 | 74 | 67 | 70 | 61 | 69 | 64 | 69 | 68 | 69 | 70 | 68 | 3 |
| Cr | 28 | 19 | 15 | 13 | 22 | 25 | 22 | 24 | 22 | 27 | 23 | 20 | 23 | 22 | 4 |
| Zn | 11 | 9 | 8 | 8 | 9 | 7 | 9 | 10 | 12 | 11 | 13 | 9 | 9 | 10 | 2 |
| Cu | 13 | 10 | 11 | 11 | 10 | 11 | 18 | 11 | 14 | 20 | 17 | 10 | 11 | 13 | 3 |
| Zr | 11 | 15 | 14 | 15 | 14 | 14 | 23 | 14 | 19 | 17 | 23 | 15 | 14 | 16 | 4 |
| Y | 29 | 33 | 35 | 37 | 34 | 35 | 31 | 35 | 32 | 29 | 32 | 34 | 35 | 33 | 2 |
| Pb | 6 | 7 | 7 | 8 | 7 | 7 | 6 | 7 | 7 | 6 | 7 | 7 | 7 | 7 | 1 |
| Nb | 31 | 28 | 29 | 31 | 29 | 30 | 27 | 30 | 28 | 27 | 28 | 29 | 30 | 29 | 1 |
| Rb/Sr | 0.13 | 0.04 | 0.05 | 0.06 | 0.05 | 0.05 | 0.05 | 0.04 | 0.04 | 0.15 | 0.04 | 0.04 | 0.05 | 0.06 | 0.04 |

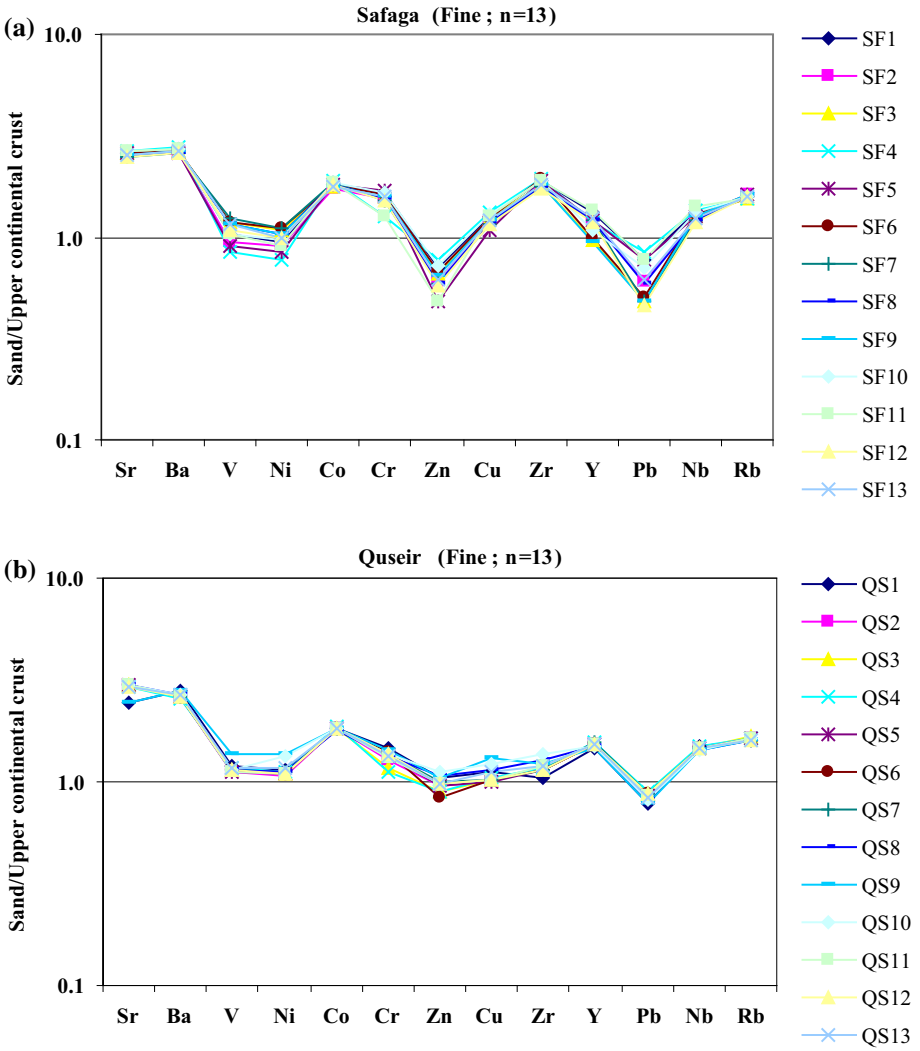


Figure 7. Multi-element normalized diagram for the coastal dune sand samples, normalized against average upper continental crust (Taylor and McLennan 1985). A horizontal line of sand/upper continental crust value of 1 is included for reference. (**a**) Safaga and (**b**) Quseir.

dune sands are less than the average PAAS (∼0.80; Taylor and McLennan 1985), suggesting low intensity of chemical weathering in the source area.

Among the hydraulic fractionation indexes, the ratio of opaque/non-opaque (O/NO) and a stability index (zircon + tourmaline + rutile/pyroxene + hornblende (ZTR/PH)) (table 2) values show significant differences among the sedimentary provinces of the two examined dune fields. The highest O/NO ratio values (0.6, table 2) were recorded at SF coastal dune sands, which indicate the effect of magmatic and metamorphic source rocks. The lowest O/NO values (0.2, table 2) were recorded at QS coastal dune sands; suggest recycled sedimentary rocks. Also, the highest values of stability index ZTR/PH (0.15, table 2) were recorded at SF coastal dune sands which indicate large transport distance and the effect of fluvial and marine processes.

The Index of Compositional Variability (ICV) values (Cox *et al.* 1995) can be used to evaluate the hydraulic sorting of sands of studied dune fields. The ICV values are higher than 0.84 for both SF and QS coastal dune sands (table 3), suggesting that the dune sands are enriched in rock forming minerals. Similarly, the high $SiO_2/Al_2O_3$ ratio values, indicates the compositional maturity of both SF and QS coastal dune sands (Armstrong-Altrin *et al.* 2015a).

The enrichment of Co within the coastal dune sand samples may be due to the recycling of sedimentary lithics near marine environments or may be associated with $TiO_2$ and $Fe_2O_3$ in rutile, ilmenite and magnetite (Zolezzi-Ruiz 2007).

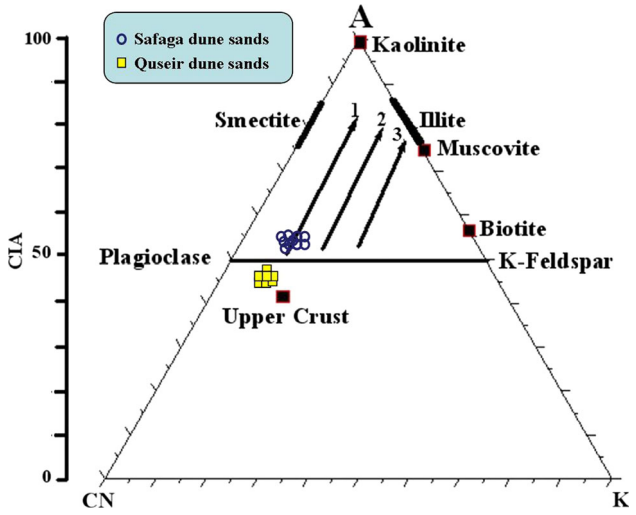


Figure 8. A–CN–K ternary diagram of molecular proportions of $Al_2O_3$–($CaO^*$ + $Na_2O$)–$K_2O$ (after Nesbitt and Young 1984). Also plotted is the average upper continental crust (Taylor and McLennan 1985), as well as some rock forming minerals important in silicate rock weathering; shown at the side is the CIA scale. Arrows 1–3 represent the weathering trends of granodiorite, adamellite and granite, respectively (Nesbitt and Young 1984).

### 5.3 *Provenance*

The discriminant function diagram (figure 5) shows that the sand samples of SF dune field are plotted mainly in the felsic igneous province, whereas the sand samples of QS dune field are plotted exclusively in the quartzose sedimentary province. This result (figure 5) indicated that the coastal dune sands are subject to many recycled episodes but not reflect the real source rock of these sands. This means that the coastal dune sands in both sites controlled by fluvial and beach sands composition rather than the main source rock composition. Some polycrystalline quartz grains consist of two-to-five or more subcrystals with slightly curved or crenulated intercrystalline boundaries which suggest the effect of metamorphic-plutonic source (Blatt *et al.* 1980), which indicate a granitic source and have the characteristics of marine formation.

The heavy mineral assemblage of the continental margins can be easily differentiated from the intraoceanic, island-arc, and deep marginal sea region by the percentage of minerals when plotted on the MF/MT/GM diagram, which was applied by Nechaev and Isphording (1993). The plotted data show that the heavy minerals association of coastal dune sands reflect divergent plate boundaries where MF>GM and GM<85% in most cases (figure 9a). On the other hand, the distribution patterns of the studied samples on ZGT diagram of Sato (1969) shows that most of the coastal dune sand samples plotted in type I along the ZT line and in between type I and II (figure 9b), which indicate the effects of plutonic-metamorphic source rocks and the fluvial and marine processes. Textural and mineralogical features of SF and QS coastal dune sands such as fine grains, moderately-sorted to well-sorted, high-percentage of sedimentary (carbonate) lithic fragments, rounded grains

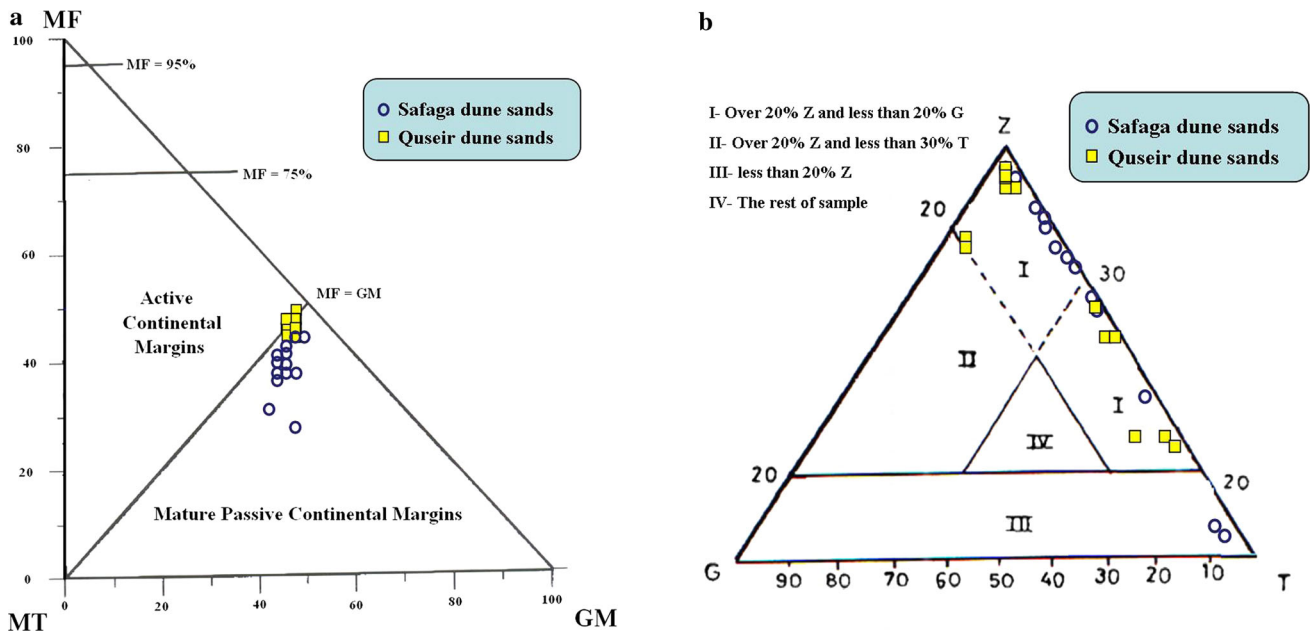


Figure 9. (**a**) Inter-relationship of the MF–MT–GM suites in beach sand along the Gulf of Suez (after Nechaev and Isphording 1993) and (**b**) ternary diagram showing distribution of ZGT percentages according to Sato (1969).

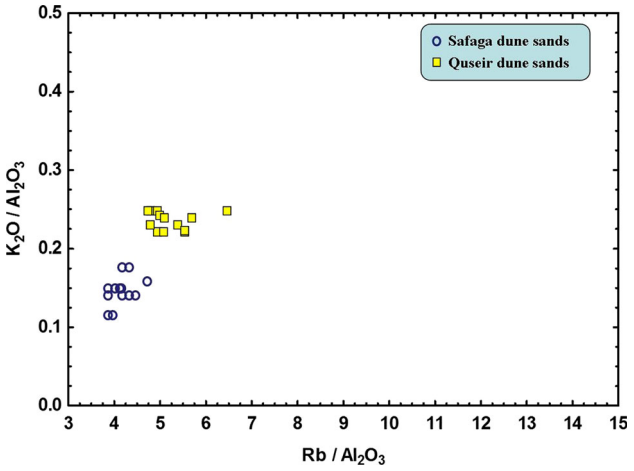


Figure 10. $K_2O/Al_2O_3$ *vs.* $Rb/Al_2O_3$ bivariate diagram for the dune sands (after Armstrong-Altrin *et al.* 2012).

of zircon and rutile, suggesting that a component of the provenance is older (pre-existing) sedimentary rocks with subordinate metamorphic-plutonic source rocks exposed near the studied dune fields (Al-Habri and Khan 2008).

The $K_2O/Al_2O_3$ *vs.* $Rb/Al_2O_3$ plot (figure 10) shows that the coastal dune sands of SF and QS are different in composition, and indicates a different source composition (Armstrong-Altrin *et al.* 2012). The SF and QS coastal dune sands have low average Cr ($36 \pm 9$, $22 \pm 4$, respectively) and Ni ($10 \pm 2$, $14 \pm 4$, respectively) contents, reflecting the absence of ultrabasic rocks in the source area (Armstrong-Altrin *et al.* 2004). This study reveals that the SF and QS coastal dune sands formed mainly from recycled sediments with subordinate metamorphic-plutonic source rocks exposed near the studied dune fields.

### 5.4 *Tectonic setting*

Verma and Armstrong-Altrin (2013) proposed two new discriminant-function-based major-element diagrams for the tectonic discrimination of siliciclastic sediments from three main tectonic settings: island or continental arc, continental rift, and collision, created for the tectonic discrimination of high ($(SiO_2)$adj = 63–95%) and low-silica rocks ($(SiO_2)$adj = 35–63%). These two new diagrams were constructed based on worldwide examples of Neogene-Quaternary siliciclastic sediments from known tectonic settings, loge-ratio transformation of ten major elements with $SiO_2$ as the common denominator, and linear discriminant analysis of the loge-transformed ratio data. Recently, these diagrams were evaluated by Armstrong-Altrin (2015) and identified a good functioning of

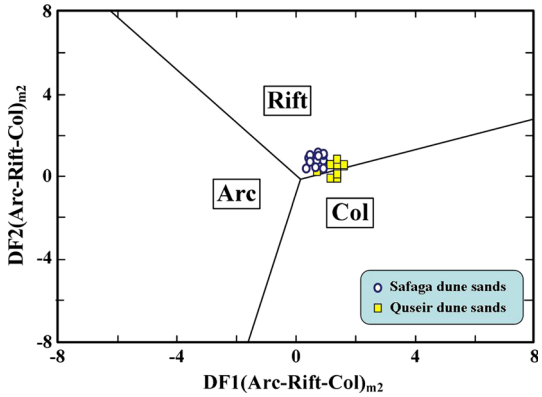


Figure 11. New discriminant-function multi-dimensional diagram proposed by Verma and Armstrong-Altrin (2013) for high-silica clastic sediments from three tectonic settings (arc, continental rift, and collision). The subscript m1 in DF1 and DF2 represents the high-silica diagram based on $\log_e$-ratios of major-elements. The discriminant function equations are:

$$DF1_{(Arc-Rift-Col)m1} = (-0.263\times \ln(TiO_2/SiO_2)_{adj}) + (0.604\times \ln(Al_2O_3/SiO_2)_{adj}) + (-1.725\times \ln(Fe_2O_3^t/SiO_2)_{adj}) + (0.660\times \ln(MnO/SiO_2)_{adj}) + (2.191\times \ln(MgO/SiO_2)_{adj}) + (0.144\times \ln(CaO/SiO_2)_{adj}) + (-1.304\times \ln(Na_2O/SiO_2)_{adj}) + (0.054\times \ln(K_2O/SiO_2)_{adj}) + (-0.330\times \ln(P_2O_5/SiO_2)_{adj}) + 1.588.$$

$$DF2_{(Arc-Rift-Col)m1} = (-1.196\times \ln(TiO_2/SiO_2)_{adj}) + (1.604\times \ln(Al_2O_3/SiO_2)_{adj}) + (0.303\times \ln(Fe_2O_3^t/SiO_2)_{adj}) + (0.436\times \ln(MnO/SiO_2)_{adj}) + (0.838\times \ln(MgO/SiO_2)_{adj}) + (-0.407\times \ln(CaO/SiO_2)_{adj}) + (1.021\times \ln(Na_2O/SiO_2)_{adj}) + (-1.706\times \ln(K_2O/SiO_2)_{adj}) + (-0.126\times \ln(P_2O_5/SiO_2)_{adj}) - 1.068.$$

these diagrams for discriminating the tectonic of setting of older sedimentary basins. Similarly, these diagrams were used in recent studies to discriminate the tectonic setting of a source region, based on sediment geochemistry (Armstrong-Altrin *et al.* 2015a; Zaid 2015c). One of these new discriminant-function based major-element diagrams (i.e., the high-silica diagram ($(SiO_2)$adj ≥63 to ≤95%, figure 11) is used in this study to identify the tectonic environment of the two investigated dune fields. This diagram (figure 11) indicated that the coastal dune sand samples of both SF and QS placed in the rift field, except five samples that plotted near the line between the collision and rift fields. These results provide a good evidence for the extension in the Red Sea rift system during Oligocene–post Pliocene, which is consistent with the general geology of Egypt (Said 1990).

Recently, Verma and Armstrong-Altrin (2016) also proposed two new discriminant-function-based multidimensional diagrams for the discrimination of active and passive margin settings. These diagrams (figure 12a, b) indicated that coastal dune

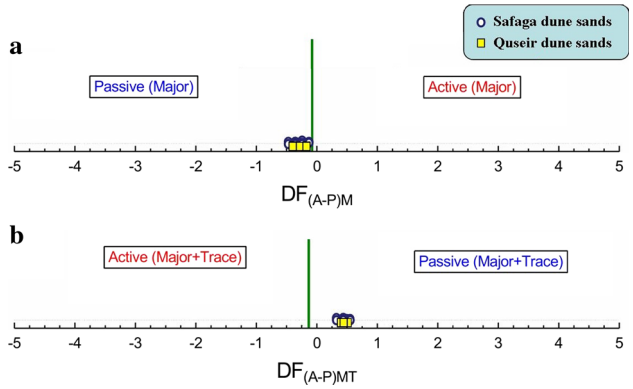


Figure 12. The new multi-dimensional discriminant function diagrams proposed by Verma and Armstrong-Altrin (2016) for the discrimination of active (A) and passive (P) margin settings. (**a**) Major element (M) based diagram and (**b**) combined major and trace element (MT) based diagram. The discriminant function equations are:
(1) $DF_{(A-P)M} = (3.0005 \times ilr1_{TiM}) + (-2.8243 \times ilr2_{AlM}) + (-1.0596 \times ilr3_{FeM}) + (-0.7056 \times ilr4_{MnM}) + (-0.3044 \times ilr5_{MgM}) + (-0.6277 \times ilr6_{CaM}) + (-1.1838 \times ilr7_{NaM}) + (1.5915 \times ilr8_{KM}) + (0.1526 \times ilr9_{PM}) - 5.9948.$
(2) $DF_{(A-P)MT} = (3.2683 \times ilr1_{TiMT}) + (5.3873 \times ilr2_{AlMT}) + (1.5546 \times ilr3_{FeMT}) + (3.2166 \times ilr4_{MnMT}) + (4.7542 \times ilr5_{MgMT}) + (2.0390 \times ilr6_{CaMT}) + (4.0490 \times ilr7_{NaMT}) + (3.1505 \times ilr8_{KMT}) + (2.3688 \times ilr9_{PMT}) + (2.8354 \times ilr10_{CrMT}) + (0.9011 \times ilr11_{NbMT}) + (1.9128 \times ilr12_{NiMT}) + (2.9094 \times ilr13_{VMT}) + (4.1507 \times ilr14_{YMT}) + (3.4871 \times ilr15_{ZrMT}) - 3.2088.$

sand samples of both SF and QS dune fields were deposited in a passive continental margin field. The results obtained from these discriminant function diagrams are consistent with the regional geology of the Egyptian Red Sea Coastal plain during the Oligocene–post Pliocene (Purser and Philobbos 1993).

## 6. Conclusions

- The SF and QS coastal dune sands are fine-size, moderately, moderately-well to well-sorted, coarse-skewed to near-symmetrical sands and mesokurtic. This reflects that the coastal dune sands inherited from the beach zone where onshore winds picked-up and transport grains into a wide Red Sea coastal plain at the border of the beach.
- The coastal dune sands of SF and QS are mainly plotted in the recycled orogen and partly in craton interior fields, suggesting recycled older sedimentary with subordinate metamorphic-plutonic sources. The mineralogical (Qt–Ft–Lt) and geochemical composition of the sands, indicate that SF and QS coastal dune sands are mature and influenced by quartz-rich sands. Major sediment supply for the coastal dune sands comes mainly from alluvial sands of the adjacent large wadis, which are enriched with quartz and sedimentary lithics.
- The Red Sea coastal dune sands suffer from arid climate and little chemical weathering (CIA values low relative to the range of the PAAS) and they are chemically homogeneous This implies that aeolian activity is partially controlling the geochemistry of the sands.
- The new tectonic discriminant-function diagrams suggest that the coastal dune sands were deposited in a passive margin of a synrift basin and provide a good evidence for the extension in the Red Sea rift system during Oligocene-post Pliocene, which is consistent with the general geology of Egypt.

## Acknowledgements

The author is greatly indebted to the members of the laboratory of the Central Metallurgical Research and Development Institute, Egypt for facilitating analytical work for the present research.

## References

Al-Habri O A and Khan M M 2008 Provenance, diagenesis, tectonic setting and geochemistry of Tawil sandstone (Lower Devonian in central Saudi Arabia); *J. Asian Earth Sci.* **33** 278–287.

Armstrong-Altrin J S 2009 Provenance of sands from Cazones, Acapulco, and Bahía Kino beaches; Mexico; *Rev. Mex. Cienc. Geol.* **26(3)** 764–782.

Armstrong-Altrin J S 2015 Evaluation of two multidimensional discrimination diagrams from beach and deep-sea sediments from the Gulf of Mexico and their application to Precambrian clastic sedimentary rocks; *Int. Geol. Rev.* **57** 1446–1461.

Armstrong-Altrin J S, Lee Y I, Verma S P, Ramasamy S 2004 Geochemistry of sandstones from the Upper Miocene Kudankulam Formation, southern India: Implications for provenance, weathering, and tectonic setting; *J. Sedim. Res.* **74** 285–297.

Armstrong-Altrin J S, Lee Y I, Kasper-Zubillaga J J, Carranza-Edwards A, Garcia D, Eby N, Balaram V and Cruz-Ortiz N L 2012 Geochemistry of beach sands along the western Gulf of Mexico, Mexico: Implication for provenance; *Chem. Erde. Geochem.* **72** 345–362.

Armstrong-Altrin J S, Machain-Castillo M L, Rosales-Hoz L, Carranza-Edwards A, Sanchez-Cabeza J A and Ruíz-Fernández A C 2015a Provenance and depositional history of continental slope sediments in the southwestern Gulf of Mexico unraveled by geochemical analysis; *Cont. Shelf Res.* **95** 15–26.

Blatt H, Middleton G and Murray R 1980 *Origin of Sedimentary Rocks*; Prentice-Hall, New Jersey, 362p.

Carranza-Edwards A 2001 Grain size and sorting in modern beach sands; *J. Coast. Res.* **17(1)** 38–52.

Carranza-Edwards A, Kasper-Zubillaga J J, Rosales-Hoz L, Alfredo-Morales E and Santa-Cruz R L 2009 Beach sand composition and provenance in a sector of the southwestern Mexican Pacific; *Rev. Mex. Cienc. Geol.* **26(2)** 433–447.

Conoco 1987 Geological Map of Egypt, Scale (1:500,000), NH 36 SW-B.S. sheet.

Cox R, Lowe D R and Cullers R L 1995 The influence of sediment recycling and basement composition on evolution of mudrock chemistry in the southwestern United States; *Geochim. Cosmochim. Acta* **59** 2919–2940.

Dar M A 1998 Mineralogy and chemistry of the mangrove vegetation in Hurghada–Quseir area, Red Sea, Egypt; M.Sc. Thesis, Faculty of Science, Suez Canal University, 225p.

Dar M A 2002 Geological bases to study the environmental defect in the marine ecosystem as a result of touristic activities in Hurghada area and surroundings. Red Sea, Egypt; Ph.D. Thesis, Suez Canal University; 2l8p.

Dickinson W R, Beard L S, Brakenridge G R, Erjavec J L, Ferguson R C, Inman K F, Knepp R A, Lindberg F A and Ryberg P T 1983 Provenance of North American Phanerozoic sandstones in relation to tectonic setting; *Geol. Soc. Am. Bull.* **94** 222–235.

Dott R H 1964 Wackes, greywacke and matrix: What approach to immature sandstone classification; *J. Sedim. Petrol.* **34** 625–632.

Egyptian Meteorological Authority, Ministry of Transportation and Communications (1996), internal meteorological reports, Cairo, 37p.

El-Taher A and Madkour H A 2013 Texture and environmental radioactivity measurements of Safaga sand dunes; *Indian J. Geo-marine Sci.* **42(1)** 35–41.

Folk R L 1966 A review of grain-size parameters; *Sedimentology* **6** 73–96.

Folk R L 1980 *Petrology of sedimentary rocks*; Hemphill Publ. Co., Texas, 159p.

Franzinelli E and Potter P E 1983 Petrology, chemistry and texture of modern river sands, Amazon River System; *J. Geol.* **91(1)** 23–29.

Fryberger S G 1979 Dune forms and wind regime; In: *A study of global sand seas* (ed.) Mckee, Prof. Pap. US Geol. Surv. 1052.5.2.5, pp. 137–169.

Hill I G, Meighan I G and Worden R H 2000 Yttrium: The immobility–mobility transition during basaltic weathering; *Geology* **28** 923–926.

Honda M, Yabuki S and Shimizu H 2004 Geochemical and isotopic studies of aeolian sediments in China; *Sedimentology* **51** 211–230.

Kassi A M, Grigsby J D, Khan A S and Kasi A K 2015 Sandstone petrology and geochemistry of the Oligocene–Early Miocene Panjgur Formation, Makran accretionary wedge, southwest Pakistan: Implications for provenance, weathering and tectonic setting; *J. Asian Earth Sci.* **105** 192–207.

Kasper-Zubillaga J J and Zolezzi-Ruiz H 2007 Grain size, mineralogical and geochemical studies of coastal and inland dune sands from El Vizcaíno Desert, Baja California Peninsula, Mexico; *Rev. Mex. Cienc. Geol.* **24(3)** 423–438.

Kasper-Zubillaga J J, Armstrong-Altrin J S, Carranza Edwards A, Morton-Bermea O and Lozano-Santa Cruz R 2013 Control in beach and dune sands of the Gulf of Mexico and the role of nearby rivers; *Int. J. Geosci.* **4** 1157–1174.

Mansour A M 1994 Cluster analysis and mineral provenance of sand dunes, Red Sea coast, Egypt; *J. Sed. Egypt* **8** 19–33.

Mansour A M 1999 Changes of sediment nature by environmental impacts of Sharm Abu Makhadeg area, Red Sea, Egypt; *J. Sed. Egypt* **7** 25–36.

Mansour A and Sediek M 1994 Cluster analysis and mineral provenance of sand dunes, Red Sea Coast, Egypt; *J. Sedim. Soc. Egypt* **2** 55–68.

Mansour A, Nawar A and Mohamed M A 1997 Recent intertidal sediments and the negative impact of human activities, Red Sea coast, Egypt; *Egypt. J. Geol.* **41(2A)** 239:272.

Mansour A, Nawar A H and Mohamed A W 2000 Shallow marine sediments, Red Sea, Egypt: Restricted distribution of coral debris; *J. Sed. Egypt* **8** 63–73.

McBride E F 1963 A classification of common sandstones; *J. Sedim. Petrol.* **33** 664–669.

McLennan S M, Hemming S, McDaniel D K and Hanson G N 1993 Geochemical approaches to sedimentation, provenance, and tectonics. In: *Processes controlling the composition of clastic sediments* (eds) Johnsson M J and Basu A, Geol. Soc. America, Special Paper, pp. 21–40.

Nechaev V P and Isphording W C 1993 Heavy mineral assemblages of continental margins as indicators of plate-tectonic environments; *J. Sedim. Petrol.* **63(6)** 1110–1117.

Nesbitt H W and Young G M 1982 Early Proterozoic climates and plate motions inferred from major element chemistry of lutites; *Nature* **299** 715–717.

Nesbitt H W and Young G M 1984 Prediction of some weathering trends of plutonic and volcanic rocks based on thermodynamic and kinetic considerations; *Geochim. Cosmochim. Acta* **48** 1523–1534.

Philobbos E R, Mansour H H and El-Shater A 1983 Some textural characteristics of recent sediments along the Red Sea coast of Egypt; *Bull. Inst. Oceanogr. Fish* **9** 20–30.

Purser B and Philobbos E 1993 The sedimentary expressions of rifting in the NW Red Sea, Egypt; *Geol. Soc. Egypt, Spec. Publ.* **1** 1–46.

Ramadan F S and Zaid S M 2013 Provenance of recent sediments along the Red Sea coast, Egypt; *Int. J. Acad. Res.* **5(2)** 38–49.

Ries A C, Shackleton R M, Graham R H and Fitches W R 1983 Pan-African structures, ophiolites and melange in the Eastern Desert of Egypt: A traverse at 26°N; *J. Geol. Soc. London* **140** 75–95.

Rollinson H R 1993 *Using Geochemical Data: Evaluation, Presentation, Interpretation*; Longman, United Kingdom, 352p.

Roser B P and Korsch R J 1988 Provenance signatures of sandstone-mudstone suites determined using discrimination function analysis of major element data; *Chem. Geol.* **67** 119–39.

Said R 1962 *The Geology of Egypt*, Amsterdam, New York, Elsevier Publ. Co, 377p.

Said R 1990 *The Geology of Egypt*, Balkema, Rotterdam, 734p.

Sato Y 1969 Geological significance of zircon–garnet–tourmaline ratio of the Paleogene sandstone of north western Kyushu, Japan; Report, Geol. Surv. Japan, No. **235,** 46p.

Taylor S R and McLennan S M 1985 *The Continental Crust: Its Composition and Evolution*; Oxford, Blackwell, UK.

Verma S P and Armstrong-Altrin J S 2013 New multi-dimensional diagrams for tectonic discrimination of siliciclastic sediments and their application to Precambrian basins; *Chem. Geol.* **355** 117–180.

Verma S P and Armstrong-Altrin J S 2016 Geochemical discrimination of siliciclastic sediments from active and passive margin settings; *Sedim. Geol.* **332** 1–12.

Wang X, Dong Z, Zhang J, Qu J and Zhao A 2003 Grain size characteristics of dune sands in the central Taklimakan Sand Sea; *Sedim. Geol.* **161** 1–14.

Zaid S M 2002 Geo-environmental study of north Marsa Alam, Red Sea, Egypt; M.Sc. Thesis, Zagazig Univ., Egypt, 280p.

Zaid S M 2015c Geochemistry of sands along the Ain Soukhna and Ras Gharib beaches, Gulf of Suez, Egypt: Implications for provenance and tectonic setting; *Arabian J. Geosci.* **8(12)** 10,481–10,496.

Zolezzi-Ruiz H 2007 Modelo Composicional de las Dunas de Bahía Sebastián Vizcaíno, México: Distribución de Tamaño de Grano, Petrografía, Geoquímica e Implicaciones de la Procedencia del Sedimento: Mexico, D.F., Universidad Nacional Autónoma de México, Tesis De Maestría, 180p.

Corresponding editor: Partha Pratim Chakraborty